11-28-2022

A nanodiamond chemotherapeutic folate receptor-targeting prodrug with triggerable drug release

Jiangtao Wu
School of Chemistry and Chemical Engineering, Shanxi University, Taiyuan

Xiangbin Du
School of Chemistry and Chemical Engineering, Shanxi University, Taiyuan

Dongmei Zhang
Taiyuan Central Hospital, Taiyuan

Jicheng Cui
Key Laboratory of Chemical Biology and Molecular Engineering of Ministry of Education, Institute of Molecular Science, Shanxi University, Taiyuan

Xiaoxia Zhang
School of Chemistry and Chemical Engineering, Shanxi University, Taiyuan

See next page for additional authors

Recommended Citation

Authors

Jiangtao Wu, Xiangbin Du, Dongmei Zhang, Jicheng Cui, Xiaoxia Zhang, Xine Duan, John F. Trant, and Yingqi Li

1   Wu, Jiangtao, et al. "A Nanodiamond Chemotherapeutic Folate

2   Receptor-Targeting Prodrug with Triggerable Drug

3   Release." *International Journal of Pharmaceutics*, vol. 630, Jan.

4   2023, p. 122432. *DOI.org (Crossref)*,

5   https://doi.org/10.1016/j.ijpharm.2022.122432.

A nanodiamond chemotherapeutic folate receptor-targeting prodrug with triggerable drug release

Jiangtao Wu[#a], Xiangbin Du[#a], Dongmei Zhang[c], Jicheng Cui[b], Xiaoxia Zhang[a], Xine Duan[a], John F. Trant[d*], Yingqi Li[a,b*]

[a] School of Chemistry and Chemical Engineering, Shanxi University, Taiyuan 030006, P. R. China

[b] Key Laboratory of Chemical Biology and Molecular Engineering of Ministry of Education, Institute of Molecular Science, Shanxi University, Taiyuan 030006, P. R. China

[c] Taiyuan Central Hospital, Taiyuan 030009, P. R. China

[d] Department of Chemistry and Biochemistry, University of Windsor, 401 Sunset Ave, Windsor ON, N9B 3P4, Canada

# These authors contributed equally to this paper.

Jiangtao Wu: wjtsxu@qq.com

Xiangbin Du: fighterdu@163.com

Dongmei Zhang: 2374499211@qq.com

Jicheng Cui: 1422133327@qq.com

Xiaoxia Zhang: 201922902017@email.sxu.edu.cn

Xine Duan: duanxe@sxu.edu.cn

John F. Trant: jtrant@uwindsor.ca ORCID: 0000-0002-4780-4968

Yingqi Li: wkyqli@sxu.edu.cn ORCID: 0000-0002-0018-0684

Statistical Summary: The text, inclusive of figure captions, stands at 6494 words. The article contains 7 figures and 2 schemes for a total of 9 graphical items. There are no tables in the text.

Data availability: All data discussed in the article is provided in the supporting information.

36 **Conflict of Interest:** The authors declare no conflicts of interest.

37 **Ethics Approval Statement:** All animal experiments were performed according to

38 protocols approved by the Radiation Protection Institute of the Drug Safety

39 Evaluation Center in China (Production license: SYXK (Jin) 2018-0005).

Abstract

Cancer chemotherapy is often accompanied by severe off-target effects that both damage quality of life and can decrease therapeutic compliance. This could be minimized through selective delivery of cytotoxic agents directly to the cancer cells. This would decrease the drug dose, consequently minimizing side effects and cost. With this goal in mind, a dual-gated folate-functionalized nanodiamond drug delivery system (NPFSSD) for doxorubicin with activatable fluorescence and cytotoxicity has been prepared. Both the cytotoxic activity and the fluorescence of doxorubicin (DOX) are quenched when it is covalently immobilized on the nanodiamond. The NPFSSD is preferentially uptaken by cancer cells overexpressing the folate receptor. Then, once inside a cell, the drug is preferentially released within tumor cells due to their high levels of endogenous of glutathione, required for releasing DOX through cleavage of a disulfide linker. Interestingly, once free DOX is loaded onto the nanodiamond, it can also evade resistance mechanisms that use protein pumps to remove drugs from the cytoplasm. This nanodrug, used in an *in vivo* model with local injection of drugs, effectively inhibits tumor growth with fewer side effects than direct injection of free DOX, providing a potentially powerful platform to improve therapeutic outcomes.

Introduction

The side effects that arise from cancer standard of care treatments can greatly harm consumers' quality of life.(Ferlay et al., 2021; Miller et al., 2019) Some of these effects are unavoidable, but many result from the internalization of highly toxic chemotherapy drugs by healthy cells, leading to the killing of non-cancerous tissues and damage to healthy organ systems. Consequently, improving drug targeting is as important as developing new therapies to improve patient's quality of life and compliance with therapeutic regimens.(Jiang et al., 2019) Targeted chemotherapeutic nanodrug delivery systems that trigger the release of their payload upon cell internalization are being developed for cancer treatment.(Lee et al., 2020; Li et al., 2017; Pérez-Herrero and Fernández-Medarde, 2015; Xu et al., 2018) These technologies exploit the low pH, abundant reduced glutathione (GSH), high levels of reactive oxygen species, and the high expression of specific membrane receptors on cancer cells.(Hong et al., 2021; Lv et al., 2018; Paris et al., 2019) For selectivity, the drug needs to be sequestered from cells until it reaches the tumor, it needs a carrier. Nanodiamond (ND), with high biocompatibility, high chemical stability, and easy surface modification, has demonstrated efficacy in sensing,(Wu et al., 2021) drug and gene delivery,(Du et al., 2020; Li et al., 2019; Yuan et al., 2021) and biological imaging,(Jung and Neuman, 2021) is a promising candidate as this carrier for drug delivery.(Cui et al., 2021; Long et al., 2020; Wei et al., 2019; Xu et al., 2021) NDs are submicron single crystal diamond with a core consisting only of sp^3 carbon atoms, passivated with a surface layer of oxidized sp^2 carbon.(Chauhan et al., 2020)

Generally, drugs are physically adsorbed onto the ND, leading to premature "burst" release that begins as soon as the material is diluted into medium. This solves the solubility problem but doesn't resolve off-target toxicity. Covalent immobilization avoids burst release, but of course requires bond cleavage. Only a few reports have explored this strategy: one with paclitaxel,(Liu et al., 2010) a multi-modal system functionalized with both antibodies and oligonucleotide-drug conjugates,(Zhang et al., 2011) and a previous example with DOX.(Zhao et al., 2014) Unfortunately, none of these conjugates has activatable cytotoxicity or activatable fluorescence to evaluate drug release when the system enters the cell. This limits the ability to characterize

localization, release, and to correlate efficacy with release kinetics. Recently, we reported a pH-responsive activatable fluorescent and cytotoxic ND system that significantly inhibited tumor growth.(Du et al., 2020) We propose that this can be refined and combined with DOX to create a new Near-IR intraoperational theranostic.(Jiao et al., 2020) Near-IR has many benefits over competing technologies as it can be used in real-time during surgery to assist in the identification of tumor margins.

GSH concentrations in tumor cells (1-10 mM) are approximately 100-1000-fold higher than those in healthy extracellular matrix and body fluids (2-10 μM).(Yang et al., 2019) More importantly, GSH levels in tumor cells are approximately 4-fold higher compared to those in normal cells. Higher intracellular GSH concentration will accelerate the cleavage of disulfide bonds,(Cheng et al., 2011) and this property has been used to modulate the stability of nanocarriers, resulting in prolonged circulation time of nanodrug-loaded particles and controlled release of intracellular molecules.(Ling et al., 2018; Tu et al., 2017) Herein we wish to disclose a targeted and intracellular activatable theranostic nanoplatform (NPFSSD) generated by covalently functionalizing ND with both DOX and folic acid (FA) (Scheme 1).
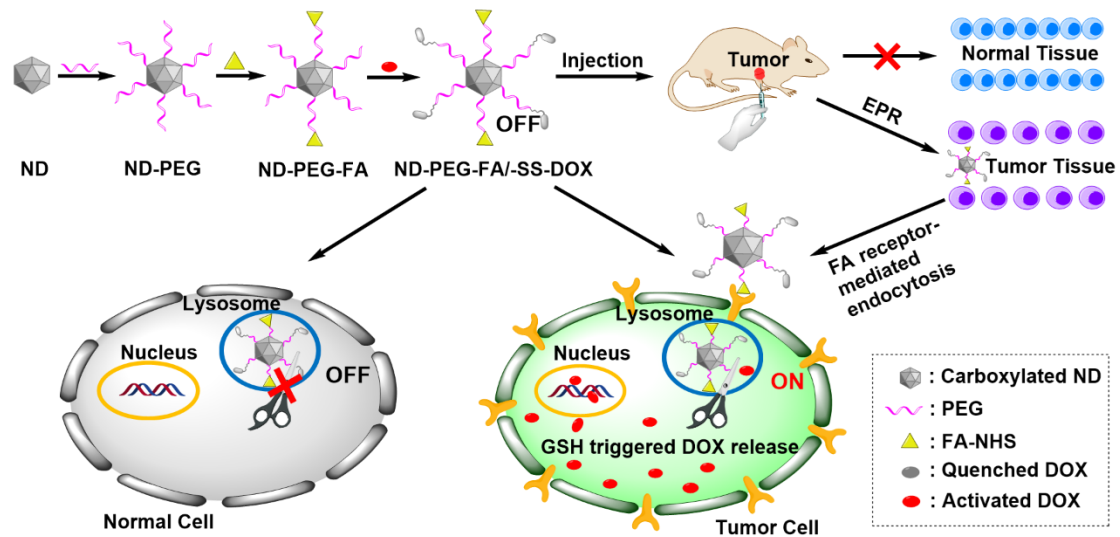
Scheme 1 An overview of the synthesis and activity of the dual-gated ND-PEG-FA/-SS-DOX (NPFSSD) nanoparticles.

Experimental

Materials and instruments

Synthetic type 1b ND powders (140 nm diameter, Element Six, Didcot UK) were carboxylated (ND-COOH) according to our previously reported method.(Dong et al., 2015) Polyethylene glycol diamine (NH$_2$-PEG-NH$_2$, M_w: 2000), N-Hydroxysuccinimide (NHS), 2-(N-morpholino)-ethanesulfonic acid (MES), Hoechst 33258, and 1-(3-dimethylaminopropyl)-3-ethyl carbodiimide hydrochloride (EDC), were purchased from Sigma-Millipore (St. Louis, USA). Doxorubicin hydrochloride (DOX), M-β-CD, and 3, 3'-dithio dipropionic acid were purchased from Shanghai Aladdin Reagent Co., Ltd (Shanghai, China). Ditert-butyl dicarbonate ester and acetyl chloride were bought from Shanghai Macklin Biochemical Technology Co., Ltd (Shanghai, China). Sodium bicarbonate, triethylamine (TEA), N, N-Dimethylformamide, and dimethyl sulfoxide were purchased from the Tianjin Dengfeng Chemical Reagent Factory (Tianjin, China). Dulbecco Minimum Essential Media (DMEM) was purchased from Thermo Fisher Biological and Chemical Product (Beijing, China). Fetal bovine serum was purchased from Hangzhou Sijiqing Biological Engineering Materials Co., Ltd (Hangzhou, China). Sucrose was purchased from the Beijing Chemical Reagent Factory (Beijing, China). The human cervical cancer cell line (HeLa), human hepatoma cancer cell line (HepG2), human liver cells (HL-7702) and mouse embryonic fibroblast (3T3) were kindly donated by the Gene Engineering Center of Shanxi University. DOX-resistant human breast cancer cell (MCF-7/ADR) were purchased from iCell Bioscience Inc. All other chemicals and solvents were of analytical grade and procured from local suppliers unless otherwise mentioned. Millipore filtered water was used for all aqueous solutions.

The UV-vis absorption spectra were carried out using a Cary 50 Bio UV-vis Spectrophotometer (Agilent, Santa Clara, CA, USA). The other data was collected on a Fourier transform infrared spectrometer (FTIR-8400S, Shimadzu Corporation, Kyoto, Japan), a Raman spectrometer (Cora 7X00, Anton Paar trading Co., LTD Shanghai, China)，a dynamic light scattering instrument (Nano-ZS90, Malvern Instruments Co., Ltd, England), a scanning electron microscope (SEM, JSM-6701F, Japan Electronics Co., Ltd), an inverted fluorescence microscope (AX10, Zeiss company, Germany), a thermostatic cell incubator (HF240, Shanghai Lishen

Scientific Instrument Co., Ltd), an inverted microscope (TS100-F, Nikon company, Germany), a fully automatic microplate reader (Model 550, Bio-Rad, USA), a flow cytometer (FACS Calibur, BD, USA), a laser scanning confocal microscope (LSM880 + Airyscan, Zeiss), an *in-vivo* small animal optical imaging system (Bruker FX pro), a real-time dynamic cell monitoring analyzer (xCELLigence RTCA S16, ACEA Biosciences), a paraffin embedding machine (Histocentre 3, Shandon, England), an automated tissue-dehydrating machine (Excelsior, Shandon, England), a paraffin slicing machine (Finesse325, Shandon, England), and an automatic biochemical analyzer (SELECTRA-E, Vertu, Holland).

Preparation of functionalized ND

ND-PEG-FA (NPF). Carboxylated ND (ND-COOH), ND-PEG-NH$_2$ (NP) and ND-PEG-FA (NPF) were prepared using our previously reported procedure.(Dong et al., 2015)

ND-PEG-FA/-SS-COOH (NPFSS)

3, 3' - dithio-dipropionic acid (DTDP, 0.5 mg) was weighed and transferred to a round bottomed flask. To this, acetyl chloride (2.0 mL) was added, and the mixture was stirred for 2 h at 65°C.(Zhang et al., 2017) After cooling to ambient, the acetyl chloride was removed under reduced pressure. Then cold ether was added to precipitate the product, 3, 3' -dithio-dipropionic anhydride (DTDPA), which was dried in a vacuum oven.

NPF (10.0 mg) was dispersed in 5 mL of sodium borate buffer solution (BBS, 0.1M, pH 8.4), and sonicated for 30 min. To this was added the freshly made 3,3 '-dithio-dipropionic anhydride (DTDPA) dissolved in 8 mL DMF dropwise. A few drops of triethylamine were also added to correct the pH to 8.4. After stirring for 12 h in the dark, ND-PEG-FA-SS-COOH (NPFSS) was isolated by centrifugation at 15,644 g for 5 min. The pellet was washed three times each with deionized water and anhydrous ethanol, respectively, and then placed in a vacuum drying oven. ND-PEG-SS-COOH (NPSS) was prepared in an identical fashion but using ND-PEG-NH$_2$ (10.0 mg) as the ND platform.

177

ND-PEG-FA/-SS-DOX (NPFSSD)

179   NPFSS (10.0 mg) was dispersed in 10.0 mL of MES buffer solution (0.1 M, pH
180   5.8) and sonicated for 30 min. Then EDC (2.0 mg) and NHS (2.5 mg) were added
181   successively into the suspension with magnetic stirring. After stirring for 6 h at room
182   temperature, the suspension was centrifuged at 15,644 g for 5 min and the supernatant
183   discarded. Next, the activated ND-PEG-SS-COOH was dispersed in 10.0 mL of
184   sodium borate buffer solution (BBS, 0.1M, pH 8.4). Doxorubicin hydrochloride
185   (DOX 1.2 mg) dissolved in DMSO (1.2 mL) was then added dropwise. Triethylamine
186   (TEA) was also added dropwise until the pH was about 8.4 (~10 μL). The mixture
187   was allowed to react for 24 h, stirring at room temperature, and protected from light.
188   Finally, the product ND-PEG-FA/-SS-DOX (NPFSSD) was obtained by
189   centrifugation at 15,644 g for 5 min, washed with deionized water and anhydrous
190   ethanol until the liquid supernatant was colorless, and then placed, protected from
191   light, in a vacuum oven. The supernatant was retained to determine DOX coupling
192   efficiency. ND-PEG-SS-DOX (NPSSD) without folate modification was designed and
193   prepared in the same fashion.

194

Characterization of NPFSSD

196   To confirm the successful synthesis of various nanoparticles，they were
197   characterized by Fourier transform infrared spectroscopy，UV-vis spectroscopy and
198   Raman spectrometry, where both ND and ND-PEG acted as the controls. The particle
199   size, zeta potential and polydispersity index (PDI) measurements were performed in
200   distilled water using a Zetasizer Nano ZS90. Measurements of nanoparticle size were
201   performed at 25°C and a scattering angle of 90º. The mean hydrodynamic diameter
202   was determined by cumulative analysis. Determination of the zeta potential was based
203   on the electrophoretic mobility of the nanoparticles in aqueous medium and was
204   performed using folded capillary cells in automatic mode. The morphology of the
205   NPFSSD and NPSSD were analyzed using scanning electron microscopy.

206

Evaluation of in vitro drug release

208   The DOX release study was carried out in dialysis bags (MWCO 3,000 Da) at

209   37 °C in PBS (0.01 M. pH 7.4, pH 5.0 with and without 10 mM GSH) with an air

210   oscillator (THZ-22, Taicang City Experimental Equipment Factory). First, three equal

211   portions of well dispersed NPFSSD suspension (1 mL) were placed in dialysis bags

212   and quickly immersed in 5 mL of the corresponding PBS solutions with a stirring rate

213   of 150 rpm at 37 °C away from any light. At the scheduled time points, 2 mL of

214   sample was withdrawn and replaced with 2 mL of fresh PBS. The amount of released

215   DOX was measured using ultraviolet measurements at 480 nm. NPSSD release was

216   likewise measured in triplicate using an identical protocol.

217

218   **Cell culture**

219   Both HeLa and HepG2 were selected as test lines as both have high endogenous

220   levels of GSH and both overexpress the folate receptor (FR). 3T3 cells and HL-7702

221   were used as healthy cell controls, with both showing low concentrations of GSH and

222   low levels of FR. All cells were cultured in a 10 cm Petri dish containing DMEM

223   supplemented with 10% FBS and 1% penicillin–streptomycin in a CO_2 incubator at

224   37 °C and passaged every 2 days using trypsin containing EDTA and PBS (pH 7.4).

225   DOX-sensitive (MCF-7) and DOX-resistant human breast carcinoma (MCF-7/ADR)

226   cells were incubated in RPMI-1640 medium with 15% FBS and 1% penicillin–

227   streptomycin in a CO_2 incubator at 37 °C and passaged every 2 days using trypsin

228   containing EDTA and PBS (pH 7.4).

229

230   **In vitro cytotoxicity of NPFSSD**

231   The cytotoxicity of NPFSSD was evaluated on HeLa, and 3T3 cells. Briefly, 5.0

232    $\times 10^3$ cells per well of the healthy or cancer cells were seeded into the 96-well plates

233   with 200 μL per well and treated with ND (69.8 μg/mL), NP (69.8 μg/mL), NPF (69.8

234   μg/mL), NPSS (69.8 μg/mL), NPFSS (69.8 μg/mL), NPSSD（57.3 μg/mL, containing

235   DOX 5 μg/mL), NPFSSD（69.8 μg/mL, containing DOX 5 μg/mL), or free DOX (5

236   μg/mL) for 24 h or 48h. After the incubation period, a CCK-8 solution (20 μL/well)

237   was added, and the cells incubated for another 1 h. The absorbance at 450 nm was

238   read using a microplate reader (Model 550, Bio-Rad, USA). In addition, the toxicity

239 of NPFSSD on HL-7702, or DOX-resistant cancer MCF-7/ADR cells was also

240 investigated using the same method as described above.

241

242 **Real-Time Cell Dynamic Monitoring**

243 Dynamic cell proliferation was monitored using a real-time dynamic cell

244 monitoring analyzer. 50 μL culture medium was added in each well of the E-Plate 16

245 test plate to measure the background impedance value to ensure that the selected wells

246 are in normal contact. Next, we added 100 μL culture medium mixed HeLa (5×10^3

247 cell/plate) suspension evenly to each well. The plate was then rested at room

248 temperature for 30 min, and then placed on the detection table (the detection table is

249 placed in the incubator in advance) for real-time dynamic cell proliferation detection.

250 After overnight measurement, we removed the E-Plate 16, discarded the culture

251 medium, and added materials or drugs of different concentrations (in DMEM) to each

252 hole along with an equal volume DMEM to the control group, and continued the

253 real-time dynamic monitoring for an additional 90 h.

254

255 **Confocal laser scanning microscopy**

256 Cellular uptake in MCF-7 and MCF-7/ADR cells was investigated qualitatively

257 by confocal laser scanning microscopy. The MCF-7 or MCF-7/ADR cells were

258 seeded in a glass-bottom dish at 1×10^4 cells per well for 24 h incubation. Then, the

259 cells were incubated with DOX and NPSSD (equivalent concentrations of 10 μg/mL)

260 for 3 h. After incubation, the culture media was removed, and the cells were washed

261 with PBS three times. The cells were then fixed with 4% paraformaldehyde and

262 stained with DAPI to mark the nucleus before being imaged by CLSM.

263

264 *In vivo* **studies**

265 *in vivo* **imaging**

266 Female BALB/c nude mice (16±0.5 g; 5–6 weeks old) were purchased from

267 Sipeifu Biotechnology Co., Ltd (Beijing, China). They were allowed to freely drink

268 and eat at 23±1℃; 39-43% relative humidity. All animal experiments were performed

269 according to protocols approved by the Radiation Protection Institute of the Drug

270 Safety Evaluation Center in China (Production license: SYXK (Jin) 2018-0005).

271 Mice were subcutaneously injected with HeLa cells (1×10^7) in the right armpit to

272 establish the animal tumor model. Fourteen days later, the tumor-bearing mice were

273 successfully established. The nude mice were randomly divided into four groups and

274 treated with NPFSSD (5mg/kg), NPSSD (5mg/kg) and free DOX (5mg/kg) by

275 intratumorally injection respectively. Saline was used as the negative control. The

276 nanodrugs NPFSSD and NPSSD were dispersed for 30 min before injection. The

277 nude mice were anesthetized at 4 h and 24 h after drug injection, to image *in vivo*.

278 Sample fluorescence images were taken under the same conditions. After 24 hours of

279 drug injection, the mice were euthanized. The heart, liver, spleen, lung, kidney and

280 tumors were dissected and placed in the *in vivo* imager for fluorescence imaging. The

281 excitation wavelength is 480 nm, the emission wavelength is 600 nm, the exposure

282 time is 10 s, and the bandwidth is 15 nm.

283

284 **Evaluation of antitumor efficacy *in vivo***

285 For the establishment of the animal tumor model, HeLa cells (1×10^6) mixed

286 with 200 μL of saline were subcutaneously injected in the right armpit. Then mice

287 were randomly divided into four groups (n = 5) for treatment with NPFSSD, NPSSD,

288 and free DOX (all DOX equivalent 5 mg/kg injected) once every 6 days by

289 intratumoral injection. The nano drugs NPFSSD and NPSSD were dispersed for 30

290 min before injection. Saline was used as the negative control. Body weight and tumor

291 volume of the mice were measured before every injection. No infection, impaired

292 mobility, or markedly reduced food consumption was observed. The tumor volume

293 was obtained according to the following equation: $V = (1/2ab^2)$ mm^3, where a is the

294 largest diameter and b is the smallest diameter. The relative tumor volume change (%)

295 was calculated according to our previous method:(Li et al., 2014)

296 Tumor volume change (%)= $[TV_{tt} - TV_{t0}]/TV_{t0} \times 100\%$

297 TV_{tt} is the tumor volume before injecting drug/saline weekly, and TV_{t0} is the

298 initial tumor volume. The saline-injected group was the control. At the end of the

299 experiment, the mice were sacrificed. Then, the tumors, hearts, livers, spleens, lungs,

300   and kidneys were excised, weighed, and photographed to evaluate the therapeutic
301   effect.

302   For the histological studies, these BALB/c nude mice were euthanized, and their
303   major organs harvested. Then, the obtained organs were fixed with 10% formalin,
304   embedded in paraffin, and sectioned at a thickness of 3~5 μm. The organ sections
305   were stained with hematoxylin and eosin (H&E) and observed using a fluorescence
306   microscope.

307

308   **Results and discussion**

309   **Preparation and characterization of ND-PEG-FA/-SS-DOX**

310   Compared with free drugs, carefully designed nano drugs can show prolonged
311   blood circulation, and increased accumulation at tumor sites. However, to truly meet
312   their promise, nanodrug delivery systems should only release their drug payload at
313   specific tumor sites rather than also in healthy tissue. Fortunately, the concentration of
314   GSH in tumor cells is several-fold that of normal cells.(Ding et al., 2021) This can be
315   exploited to construct a GSH-activated drug-releasing nanomedicine.

316
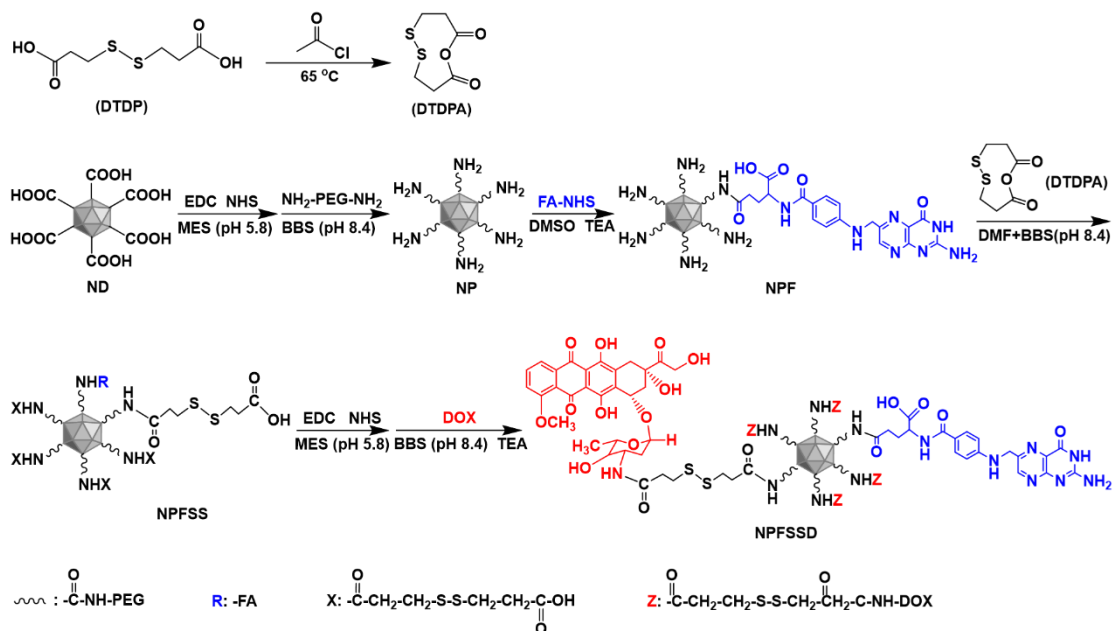
317   **Scheme 2** The synthetic scheme for preparing NPFSSD.

318   To develop a GSH-responsive drug release and targeting tumor ND system,
319   suitable surface modification on the ND is essential (Scheme 2). First, the ND was
320   functionalized with PEG-NH$_2$ (ND-PEG) to provide terminal amino groups. Then,

321 folate was added to the amines using the NHS-activated ester to obtain NPF. The

322 remaining amino groups react with DTDPA to obtain a cleavable disulfide linker

323 (ND-PEG-FA/-SS-COOH, NPFSS). Finally, the carboxyl groups of NPFSS were

324 conjugated to DOX via its amine group to provide NPFSSD. Meanwhile,

325 ND-PEG-SS-DOX (NPSSD) without FA modification was also prepared using a

326 parallel method leaving out the folate conjugation.

327   The successful synthesis, and the presence of DOX and folic acid on the surface

328 was confirmed using FT-IR (Fig. S1), Raman (Fig. S2), and UV-vis spectroscopy (Fig.

329 S3). Please see the text in the supporting information for an extended discussion of

330 the interpretation of this data. The coupling efficiency of FA was calculated by UV-vis

331 absorption. (See Fig. S4) According to the standard curve, the folic acid content in

332 NPF was calculated to be 14.8 ± 2.0 μg·mg^{-1}. The DOX coupling efficiency was

333 calculated by the formula: $DOX_{\varepsilon480nm} = 11500$ cm^{-1}·mol^{-1}·L^{-1}; meaning that DOX

334 content in ND-PEG-FA/-SS-DOX was 71.6 ± 4.2 μg·mg^{-1}, the ND-PEG-SS-DOX is

335 87.3 ± 5.1 μg·mg^{-1}.

336   Scanning electron microscopy (SEM) was used to further verify synthesis (Fig.

337 S5). The surfaces of NPSSD and NPFSSD are adopt a "fluffier" appearance than the

338 native NDs; this is consistent with surface modification. Dynamic light scattering

339 (DLS) analysis was performed to measure the particle size and zeta potential (Table

340 S1). DOX release is only 0.85% after 300 days (Fig. S6), which showed the excellent

341 stability. Furthermore, concentrated NPFSSD only begins to settle from solution

342 beyond 1 hour after mixing, suggesting a good degree of colloidal stability in PBS

343 (Fig. S7), suitable for *in vivo* applications.
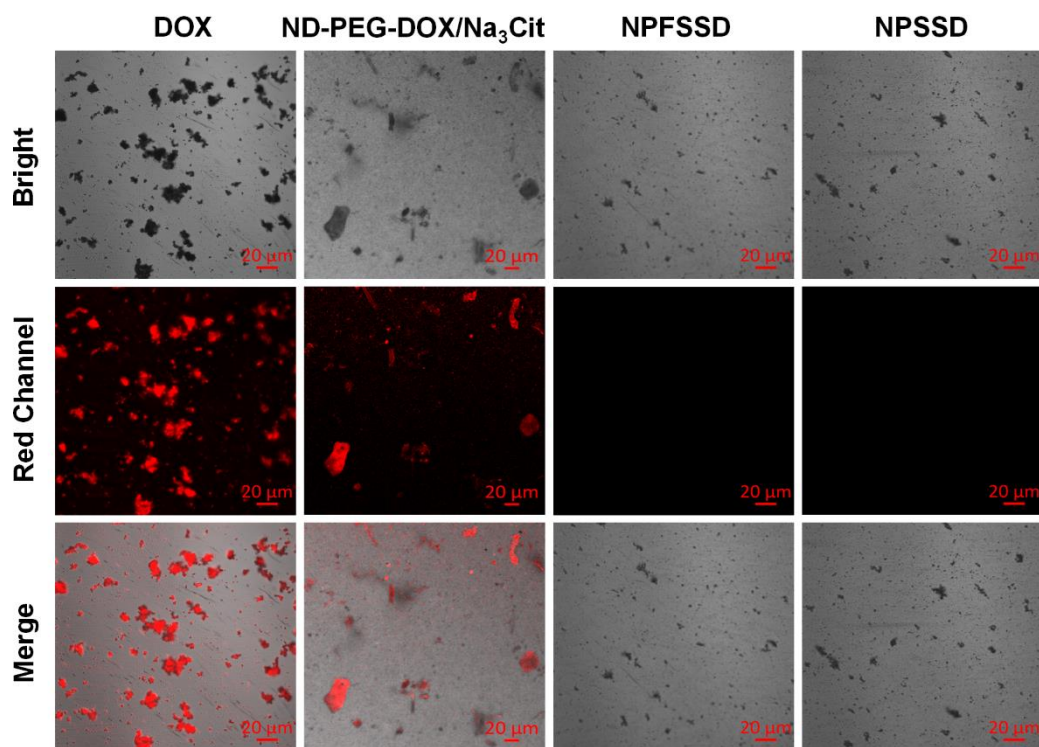
Fig. 1 Images of DOX, ND-PEG-DOX/Na₃Cit (DOX was physically adsorbed to ND-PEG in Na₃Cit medium, prepared by our previously published method),(Li et al., 2016) NPFSSD, and NPSSD under a confocal laser microscope. (Note: solid powder of DOX, suspension of ND-PEG-DOX/Na₃Cit, NPFSSD and NPSSD are dried from deionized water)

Powders of the synthesized nanomaterials and drugs were compared under daylight (Fig. S8). Compared with ND, both NPSSD and NPFSSD are red, supporting the presence of DOX. However, in contrast with free DOX, the characteristic red DOX fluorescence of NPSSD and NPFSSD is clearly quenched upon conjugation under ultraviolet light. Moreover, the red fluorescence of both free DOX and ND-PEG-DOX nanoparticles with physically-adsorbed DOX are obvious using confocal laser scanning microscopy (Fig.1),(Li et al., 2016) while the red fluorescence is completely quenched in the covalent conjugates NPFSSD and NPSSD. This quenching phenomenon is similar to the reported system,(Santra et al., 2011) where a fluorescence resonance energy transfer mechanism was ruled out.

In vitro drug release

To verify whether the NPSSD and NPFSSD systems demonstrate GSH-responsive drug release, *in vitro* drug release studies in three different media

15

363 (0.01M PBS buffer pH 7.4; 0.01M PBS buffer pH 5.0; and 0.01M PBS buffer pH 5.0

364 containing 10 mmol GSH) were conducted (Fig. 2A). We found that NPSSD and

365 NPFSSD release almost no drug at pH 7.4. At pH 5.0, NPSSD's drug release was only

366 4.84%, and that of the NPFSSD was only 3.83%, after 70 hours. Most of this release

367 occurs as a burst release in the first 10 hours, and does not meaningfully increase

368 further, indicating that release could not readily be triggered by pH. This suggests that

369 the endosomal/lysosomal acidic microenvironment alone is not enough to induce drug

370 release of either NPSSD or NPFSSD. Excitingly, when 10 mM GSH was added to the

371 PBS (pH 5.0) buffer solution, the drug release rate of both nanomedicines was

372 significantly increased, with NPSSD and NPFSSD releasing 55.27% and 58.05% of

373 the loaded DOX after about 40 hours, respectively. It was confirmed that NPFSSD

374 and NPSSD can release DOX in a slightly acidic environment rich with GSH,

375 suggesting that NPSSD and NPFSSD have potential applications in controlled drug

376 release at tumor sites.
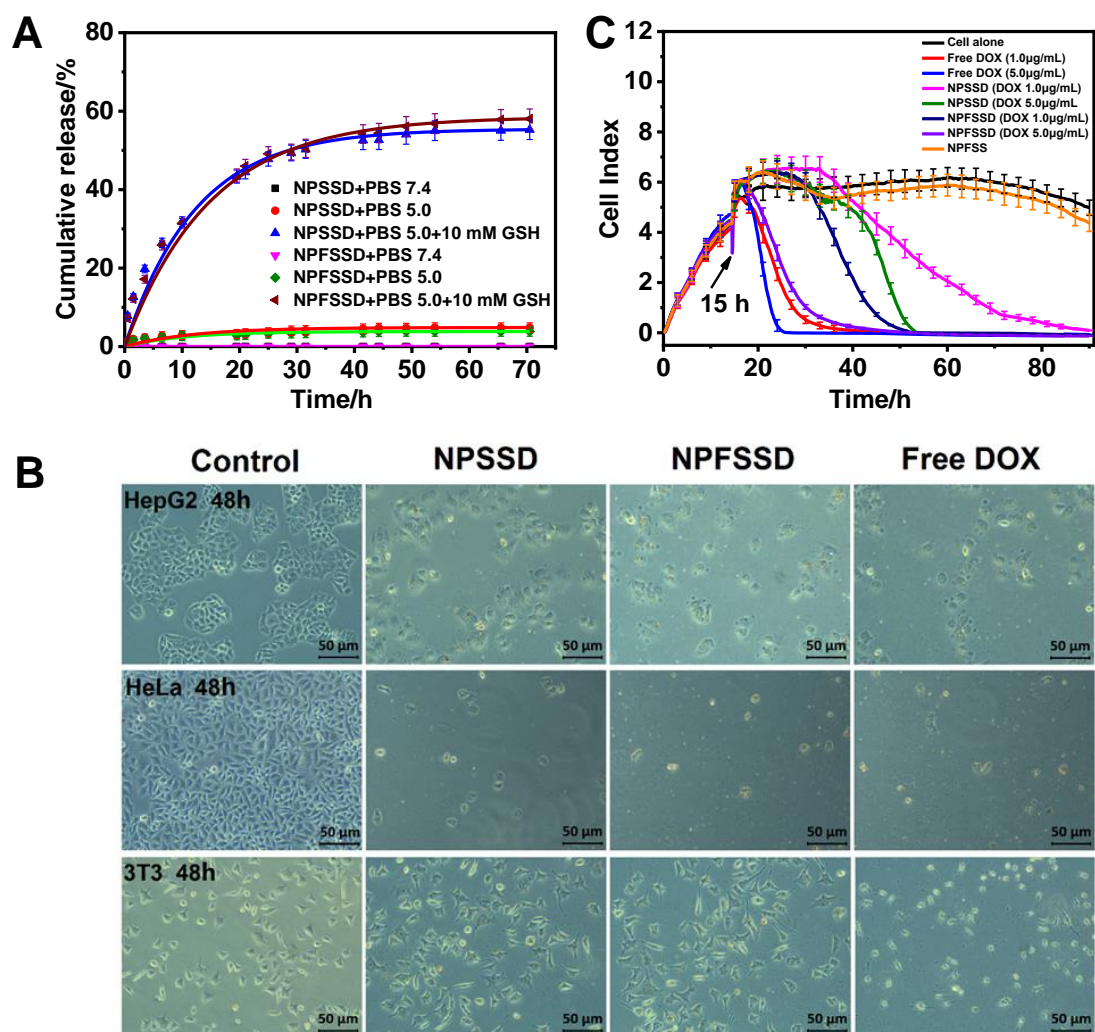
Fig. 2 (A) The *in vitro* drug release curve of both the NPFSSD and NPSSD nanomedicines; (B) Morphological changes of cells treated with various nanoparticles for 48 h. Scale bars: 50 μm; (C) The proliferation of HeLa cells treated with the different nanoparticles was monitored by real-time dynamic monitoring for 90 h.

Selective cytotoxicity of NPFSSD

Next, we investigated the effect of nanomedicine on cell number by fluorescence microscopy (Fig. 2B). Free DOX is lethal to all cells, while the nanomedicines only show activity against HeLa and HepG2. This is because NPFSSD and NPSSD require GSH cleavage in cells to release drugs. With low endogenous GSH, NPFSSD and NPSSD have little effect on 3T3 cells. In addition, CCK-8 experiment for HL-7702 cells as normal cells also showed that the NPFSSD had little toxicity to HL-7702

17

391   (Fig.S9). This result confirms that NPFSSD can use the difference in endogenous

392   GSH and surface FA receptors content between tumor cells and normal cells to kill

393   tumors selectively.

394   To further investigate the real-time effect of NPFSSD on tumor cells, the cell

395   index (CI) was quantified using a cell real-time dynamic monitoring analyzer. The CI

396   is directly proportional to the number of living cells at time relative to the total initial

397   cell count at t_0. The growth curves of HeLa cells treated with various nanomaterials

398   were obtained (Fig. 2C). All curves fluctuate greatly at 15 h, indicated with the black

399   arrow. This is the time where the culture plate is removed from the incubator for the

400   addition of the treatment to the cells, disturbing growth. The growth curve of the

401   HeLa cells without any treatment follows the usual exponential model, and the CI is

402   that of a typical cell proliferation process with limited resources. When 1.0 mg/mL of

403   the DOX-free NPFSS nanocarrier is added to the HeLa cells, the CI falls slightly

404   between 22 h to 24 h, but then it resumes normal plateau-stage behaviour. This may

405   reflect cleavage of the disulfide bond on NPFSS by GSH in HeLa cells, slightly

406   disrupting ideal proliferation. But the effect is minor, and without DOX, the ND do

407   not have a meaningful detrimental impact on the cells. This result is consistent with

408   the results of the CCK-8 test (Fig. S10), which shows obvious toxicity to tumor cells,

409   but basically no toxicity to normal cells, indicating that the nanomedicine system has

410   tumor-selective toxicity.

411   Free DOX and NPFSSD at the higher DOX concentration (5.0 $\mu g \cdot mL^{-1}$)

412   basically have the same inflection point for tumor suppression, but the CI of DOX is

413   slightly lower than that of NPFSSD (Fig. 2C), which can be ascribed to different cell

414   entry. The former is a passive diffusion into the cell and fast migration into the

415   nucleus,(Li et al., 2016) and the latter is mainly through caveolin-mediated

416   endocytosis (Fig. S11); elevated GSH levels in tumor cells favor drug release. At the

417   same DOX concentration, NPFSSD is just as toxic but the onset is delayed,

418   supporting our contention that GSH must, and can, cleave the drug from the carrier in

419   cell, and not only in cell-free *in vitro* studies. These NDs, like those previously

420   reported in the literature,(Liu et al., 2007; Ma et al., 2020; Wang et al., 2022) have

421   little inherent toxicity and are apparently highly biocompatible.

422   The targeting benefit of the folate acid functionalities was also determined by

423 flow cytometry (Fig. S12 and S13). The rate constant of NPFSSD entering the HeLa

424 cells was 0.2286 h^{-1}, while that of NPSSD was 0.1914 h^{-1}. The faster uptake rate of

425 NPFSSD supports that the folic acid-folate receptor interaction improves targeting,

426 although this is less rate discrimination than we were hoping to see.

427

428 **Confocal fluorescence microscopy imaging**

429   To provide additional support demonstrating that NPFSSD can exploit the

430 differences in GSH and surface FA receptor content between cancerous and healthy

431 cells, we employed laser confocal microscopy. As shown in Fig. 3A, when healthy (i.e.

432 low FR, low GSH) 3T3 cells were treated with NPFSSD, almost no fluorescence

433 signal is observed. In contrast, HeLa cells treated with NPFSSD exhibited strong

434 green fluorescence in their cytoplasm. This is due to the difference in intracellular

435 GSH, which cleaves the disulfides of NPFSSD to release DOX and restore the

436 fluorescence of DOX.

437   But it is not only the GSH that is important: whether we employed either NPSSD

438 nanodrug (Fig. 3D), lacking folic acid, or if we saturate the cellular media with free

439 folate before adding NPFSSD (Fig 3C), only negligeable fluorescence was observed.

440 This strongly supports our contention that folate-mediated endocytosis is extremely

441 important for cellular uptake. The targeting ability of NPFSSD for the folate receptor

442 was quantitatively analyzed by flow cytometry (Fig. S12) to measure the impact that

443 different concentrations of free folic acid have on inhibiting uptake, and on the

444 differential uptake of different cell lines. The amount of NPFSSD entering HeLa cells

445 is three times that of entering 3T3 cells, but approximately the same as that of

446 entering HepG2 cells (Fig. S12). NPFSSD exploits folate receptor-mediated

447 endocytosis to enter cells, and the rate is dependent on the available folic acid

448 receptors on the cell surface as uptake can be inhibited in a dose dependent fashion

449 with exogenous folic acid added.

450   These tools can also be used to demonstrate that release is prolonged: free DOX

451 is primarily localized in the nucleus after 1 hour incubation in Fig. 3E, while NPFSSD

452 samples still show fluorescence in the cytoplasm at 15 hours (Fig S14A). This
453 indicates that NPFSSD exhibits sustained drug release.
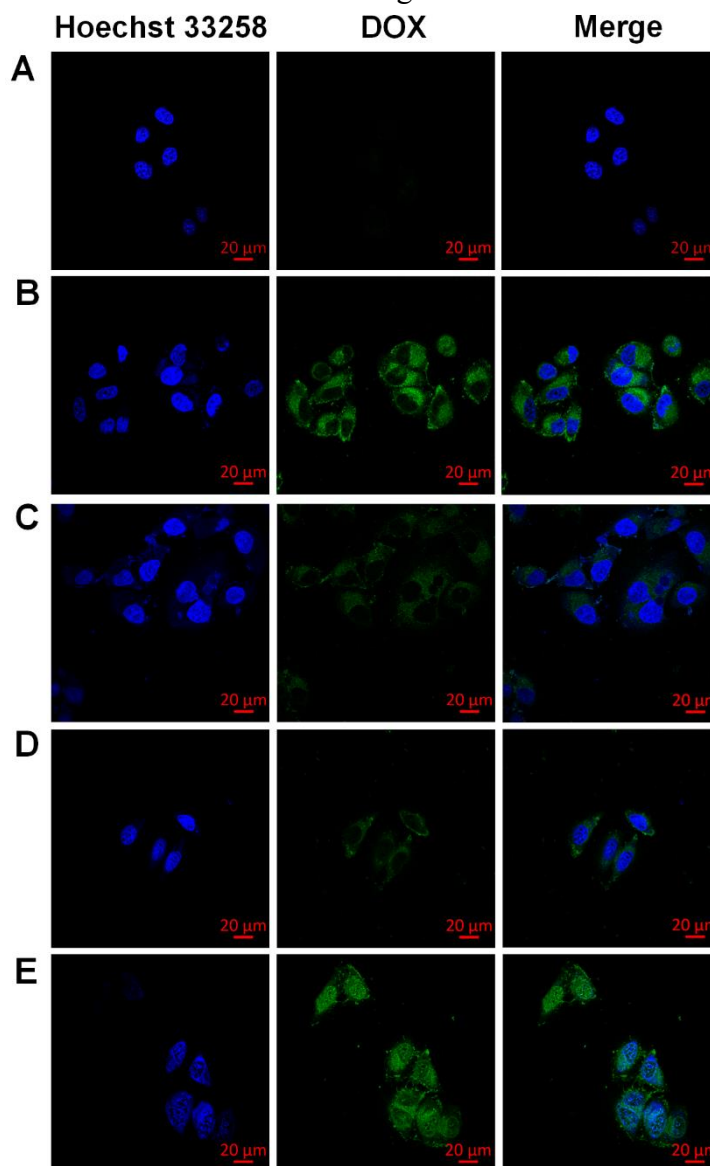
454
Fig. 3 Confocal laser scanning imaging for observing targeting of NPFSSD. (A) 3T3 cells
/NPFSSD for 3 h; (B) HeLa cells/NPFSSD for 3 h; (C) HeLa/NPFSSD+FA for 3 h; (D)
HeLa/NPSSD for 3 h; (E) free DOX for 1 h.

458 As time progressed, the fluorescence of DOX in the cytoplasm gradually was
459 increased as more NPFSSD enters the cells, allowing for disulfide cleavage, drug
460 release, and fluorescence recovery and enhancement (Fig.S14A). To determine the
461 distribution of both NPFSSD and NPSSD in the cells, a cell localization experiment
462 was carried out (Fig. S14B). A red fluorescent probe was used to label the lysosomes,
463 and the green-fluorescent signal arises from DOX released from either NPFSSD or
464 NPSSD. The results allowed us to determine that the positioning coefficients of the

particles were a similar 0.7 and 0.75 respectively, indicating that both localize to the lysosome. It also helps explain the effectiveness of NPFSSD release as GSH is highly concentrated to the lysosome. The drug then escapes the organelle and migrates into the nucleus to inhibit topoisomerase, blocking DNA reproduction.

Reversal of drug resistance to MCF-7/ADR

All the above experiments were conducted on cell lines known to be sensitive to DOX. We also wanted to investigate the potential of this nanomedicine in a DOX-resistant cancer cell line. Both response to, and the fate of, the drug, for both the sensitive MCF-7, and the closely related resistant MCF-7/ADR, was monitored using confocal microscopy (Fig. 4A and 4B). The DOX fluorescence signal in MCF-7 is very strong and mainly located in the nucleus. In the MCF-7/ADR cells, almost no fluorescence is observed, as free DOX was pumped out of the cells through P-glycoprotein (P-gp) transporters.(Zhao et al., 2020) The DOX signal of the ND drug on MCF-7/ADR cells was significantly stronger than that of free drug group We propose this difference is due to the different mechanism of drug entry into the cell and location of the drug: free DOX enters the cells through free diffusion, and binds to the P-gp protein on the membrane of cancer cells, and is rapidly pumped out by overexpressed P-gp.(Mirzaei et al., 2022) The nanodrugs enter cells by endocytosis and the DOX release is internal and away from the membrane, the DOX is then rapidly localized to the endoplasmic reticulum where it assists in the generation of reactive oxidative species that drive apoptosis.(Mirzaei et al., 2022) This suggests that where in the cell a drug is released could address resistance provided by the upregulation of membrane transporters.
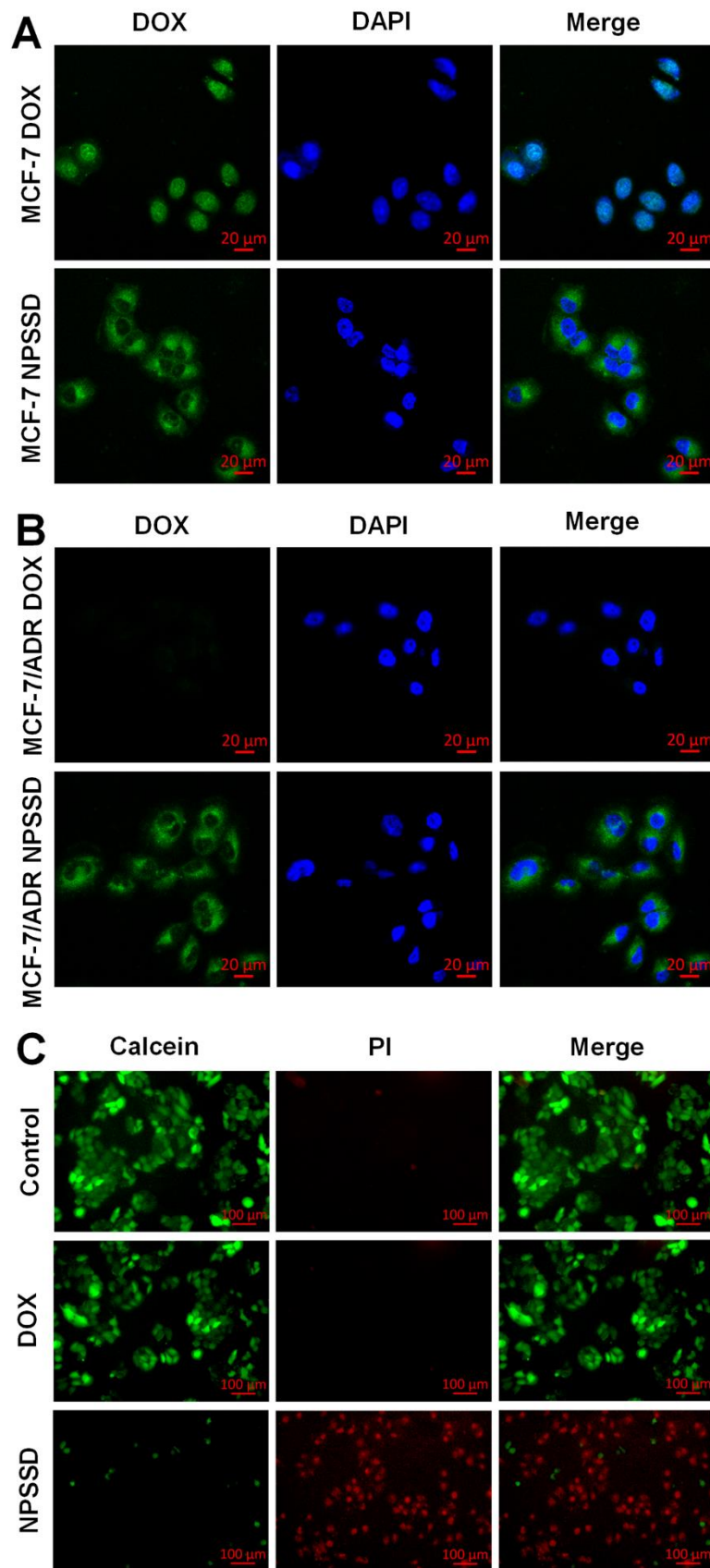
Fig. 4 Laser confocal images of (A) MCF-7; and (B) MCF-7 /ADR cells treated with NPSSD and DOX; (C) The toxicity of NPSSD to MCF-7/ADR as measured by Calcein/PI staining (48h).

492   The toxicity of the nano drugs to MCF-7/ADR was studied by a CCK-8

493   experiment. Both DOX and NPSSD kill MCF-7 cells, with the nanodrug exhibiting a

494   slower-release than the free drug (Fig. S15A). It is in the resistant strain that we see a

495   large difference: MCF-7/ADR cells incubated with DOX (100 μg/mL) over 72 hours

496   have an inhibition rate of only 37%; however, incubation with NPSSD (at a lower

497   effective DOX dose of 60 μg/mL), the inhibition rate reaches 93% (Fig. S15B). Such

498   a result suggests that NPSSD can overcome drug resistance. The IC_{50} can be

499   calculated (Table S2), and from this data the reverse drug resistance index can be

500   determined.(Zhao et al., 2020) The reverse drug resistance index of NPSSD was 7.99,

501   suggesting that nanodrugs can reverse drug resistance effectively.

502   The cytotoxicity of NPSSD on MCF-7/ADR cells was also observed by

503   Calcein/PI staining. Live cells were stained green by calcein and dead cells were

504   stained red by PI. The action time is 48 hours. Free DOX (50 μg/ mL) killed almost

505   no MCF-7/ADR cells over the 48 hours; the data resembles that of the vehicle-only

506   control group (Fig. 4C). Treatment with NPSSD (DOX equivalent 50 μg/ mL),

507   however, led to the death of most of the cells over the 48 hours (Fig. 4C). This

508   experiment further supports our contention that NPSSD negates the MCF-7/ADR

509   cells defense mechanisms against DOX and is consistent with the conclusion of the

510   CCK-8 study.

511

512   **NPFSSD and NPSSD remain localized to the tumor *in vivo***

513   The cell assays show the potential of these nanodrugs, but there can be many

514   complications that prevent an effective *in vitro* candidate from being useful *in vivo*. To

515   examine the relevance, safety, and targeting of NPFSSD and NPSSD, we used nude

516   mice in which we had established an artificial HeLa tumor. The two nanodrugs, and

517   DOX as a positive control, were injected intratumorally, the fluorescence in the living

518   mice monitored in real-time, and the tissue examined after sacrifice. The drugs were

519   dispersed in saline, and saline was used as a vehicle only control. After 4 hours

520   residence no fluorescence in any of the organs or the tumor was observed in the

521   vehicle-only saline group, confirming there is no background fluorescence in the mice

522   that competes with the signal (Fig. 5A). At 4 hours in the treatment groups, the

23

523   fluorescence signal was weak for both NPFSSD and NPSSD group in tumor site,

524   while the free DOX signal was strong at the tumor site injection. After 24h, the

525   fluorescence signal in the NPFSSD group was stronger than NPSSD group, we

526   speculate that the folate receptor-targeting of NPFSSD facilitates entry into the cancer

527   cells, and leads to greater release *via* lysosomal GSH, while more of the NPSSD

528   remains in the extracellular matrix where the DOX cannot be as easily liberated. The

529   mice were euthanized at 24 h, and *ex vivo* imaging of the heart, liver, spleen, lung,

530   kidney, and tumors was conducted (Fig. 5B). No fluorescence is observed in the saline

531   control. The representative member of the free DOX-treated group shows migration

532   of the drug to the kidneys, and especially to the liver. This can, of course, lead to

533   toxicity and the challenges with off-target effects inherent to chemotherapeutics.

534   However, in both nanodrug cases, there is no migration of fluorescence away from the

535   tumor site. At 24 hours, the NPFSSD sample is far brighter than the NPSSD sample;

536   again, this is due to faster release in the former as it better enters the cells. The drug is

537   released primarily inside the cells and does not permeate into other organs; nor can

538   the ND apparently readily migrate around the body to any significant degree, or have

539   their drug rapidly released by the lower GSH levels in non-cancerous tissue.
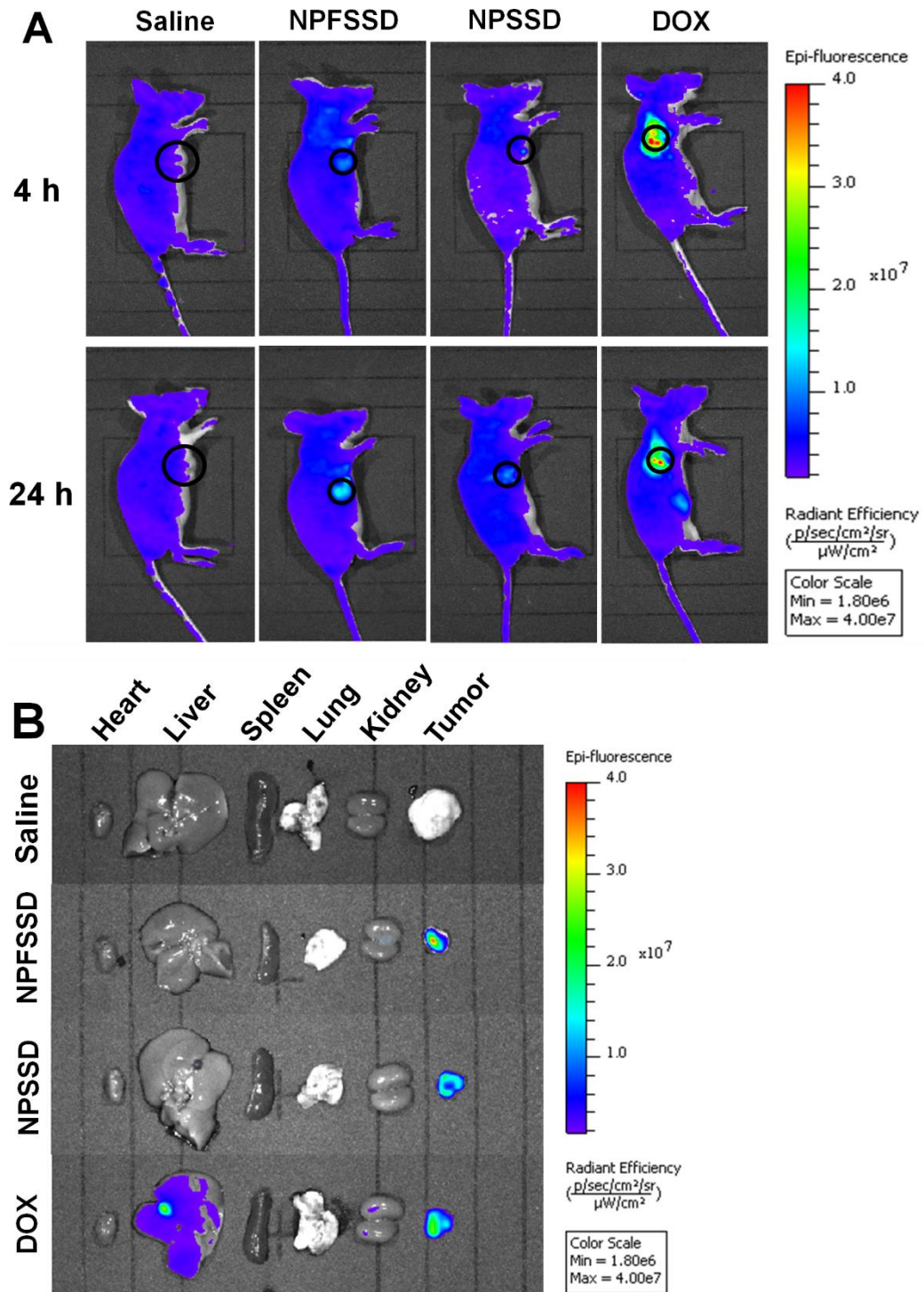
Fig. 5 (A) Representative *in vivo* fluorescent images of mice from the control and each treatment group at 4 and 24 h post intratumoral injection: the black circle highlights the location of the tumor; (B) Representative *ex vivo* superimposed fluorescent and brightfield images of the organs and tumor from each control and treatment group.

Antitumor effect *in vivo*

547　　　To evaluate the antitumor effect of NPFSSD and NPSSD *in vivo*, mice with

548　established HeLa tumors were treated with NPFSSD, NPSSD, and free DOX (dosing

549　of all subjects at a DOX equivalent of 5 mg/kg, intratumorally injected every six days

550　for 40 days, or saline vehicle set as the negative controls). The saline group chowed

551　uninhibited tumor growth, defined by excised tumor weight after sacrifice at 40 days.

552　The NPFSSD, NPSSD and free DOX groups all exhibited significant tumor inhibition

553　in Fig. 6A-C. However, the group dosed with free DOX saw very significant weight

554　loss over the study period (Fig. 6D), this is similar to the DOX-related toxicity

555　observed by others using tail vein injection and intraperitoneal injection.(Cui et al.,

556　2021; Du et al., 2020; Li et al., 2016) Free DOX clearly shows the same effects on the

557　body regardless of location of injection, expected as it can freely diffuse throughout.

558　Fortunately, the weight of the mice injected with the NPFSSD or NPSSD (and those

559　with the growing tumor in the saline group) increased gradually over time. This is

560　consistent with a far less harmful side effect profile. NPFSSD and NPSSD show high

561　efficacy against the tumor with low attendant toxicity to other systems.
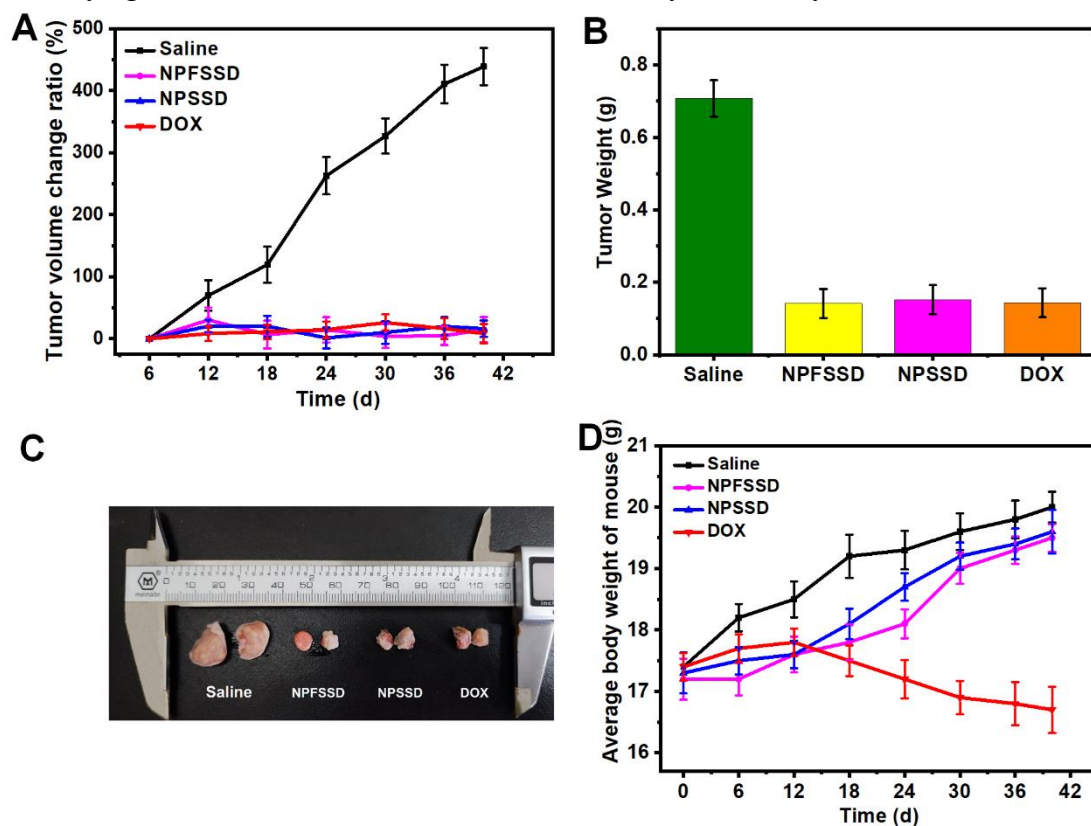
562

563　**Fig. 6** *In vivo* antitumor effects of NPFSSD and NPSSD compared to free DOX and vehicle

564　control. (A) Average tumor volume as a function of time for mice treated with saline, NPFSSD,

565   NPSSD and DOX, measured every 6 days; (B) Tumor weight for mice treated with saline,

566   NPFSSD, NPSSD and DOX on day 40 after sacrifice; (C) Representative images of the tumors 40

567   days after initial treatment; (D) Average whole mice weight analysis of the treatment groups over

568   the study.

569

570   Furthermore, the organ indices were quantified from the sacrificed animals on

571   day 40 to determine the presence of toxicity to organs according to reported

572   literature.(Du et al., 2020) A lower index indicates atrophy or reduced function, while

573   a higher index indicates blockage, swelling or impaired function.(Du et al., 2020)

574   Compared with healthy mice (no tumor, no treatment), NPFSSD and NPSSD had no

575   significant effects on heart, liver, spleen, lung or kidney, while DOX is more toxic to

576   the liver (Fig. S16). NPFSSD effectively reduces toxicity, consistent with our

577   previously reported conclusions(Du et al., 2020; Li et al., 2016; Wei et al., 2019).

578   The potential *in vivo* toxicity of nanomaterials is a major concern in the

579   nanomedicine community, and is often overlooked in studies that focus only on

580   efficacy.(Rahdar et al., 2020) In order to further investigate the safety of NPFSSD, we

581   carried out blood biochemistry analysis. Hepatotoxicity was evaluated using the liver

582   biomarkers aspartate aminotransferase (AST), alanine transaminases (ALT), alkaline

583   phosphatase (ALP) and total protein (TP) in the blood. Elevated levels can arise due

584   to damage to the liver integrity, and a leakage of the enzymes into the blood. Serum

585   AST and ALT levels in both the free DOX and saline-treated mice (damage from the

586   growing tumour) were significantly beyond the normal values observed in healthy,

587   cancer-free mice (Fig. S17), while there was a statistically insignificant elevation in

588   serum AST and ALT levels in the mice treated with either NPFSSD or NPSSD.

589   Similarly, elevated creatinine (CR) and blood urea (UREA) levels are primary

590   indicators of renal disfunction. The free DOX group shows nephrotoxicity with

591   significant elevations in both CR and UREA levels, whereas the NPFSSD and NPSSD

592   treated mice showed no significant elevation in these parameters. There is no gross

593   hepatic or renal toxicity observed during nanodrug treatment: the off-target toxicity of

594   DOX can be reduced by covalently coupling DOX onto ND without sacrificing

595   antitumor efficacy.

In addition to the biochemical assays, the *in vivo* toxicity of NPFSSD was also evaluated through histological analysis of the major organs and tumor (Fig. 7). Both the nanodrugs and free DOX elicited tumor tissue fibrosis, cell transformation, calcification, and cavitation, suggesting both kill tumor cells. These histological effects are consistent with DOX effects reported in the literature.(Ashrafizadeh et al., 2022; Nicoletto and Ofner, 2022; Norouzi et al., 2021; Sonju et al., 2022) In addition, in the ND-treated samples, we clearly observe gray ND aggregates accumulating in the tumor slices (oval marked in Fig. 7). Isolation of these residues and Raman analysis identified this as ND-PEG-FA/-SH, the residual material left one the DOX is released from NPFSSD (Fig. S18). This residue is not visible in any other tissue, which is consistent with our localization of the fluorescence to the tumor alone in the imaging study and with the low toxicity of the nanodrugs on the organs. Compared to the organs of healthy mice, those of mice injected with free DOX demonstrate liver cell cytoplasm vacuole degeneration, granular degeneration, and focal point necrosis of the liver cells (as indicated by the black arrow). The heart sections of these DOX-treated mice show minor degeneration of myocardial fibers and the beginnings of interstitial edema. Both the glomerular volume and number of glomeruli decrease slightly in the kidney, and abnormal renal tubules form. Spleen sections show red pulp atrophy and an enlargement of the white pulp, accompanied by noticeable deposition of hemosiderin. There are no distinct lung abnormalities. In contrast to this multiple organ damage elicited by treatment with this 5 mg·kg^{-1}, admittedly high, dose of free DOX, the mice treated with the same nominal DOX dose but in the form of the nanodrug exhibit no obvious organ toxicity in any of the examined organs. This is completely consistent with all the other data reported here: free DOX diffuses throughout the body, while the nanodrugs remain localized to the tumour site, leading to no observable off-site effects.

	Heart	Liver	Spleen	Lung	Kidney	Tumor
A	100 μm	100 μm	100 μm	100 μm	100 μm	
B	100 μm	100 μm	100 μm	100 μm	100 μm	100 μm
C	100 μm	100 μm	100 μm	100 μm	100 μm	100 μm
D	100 μm	100 μm	100 μm	100 μm	100 μm	100 μm
E	100 μm	100 μm	100 μm	100 μm	100 μm	100 μm
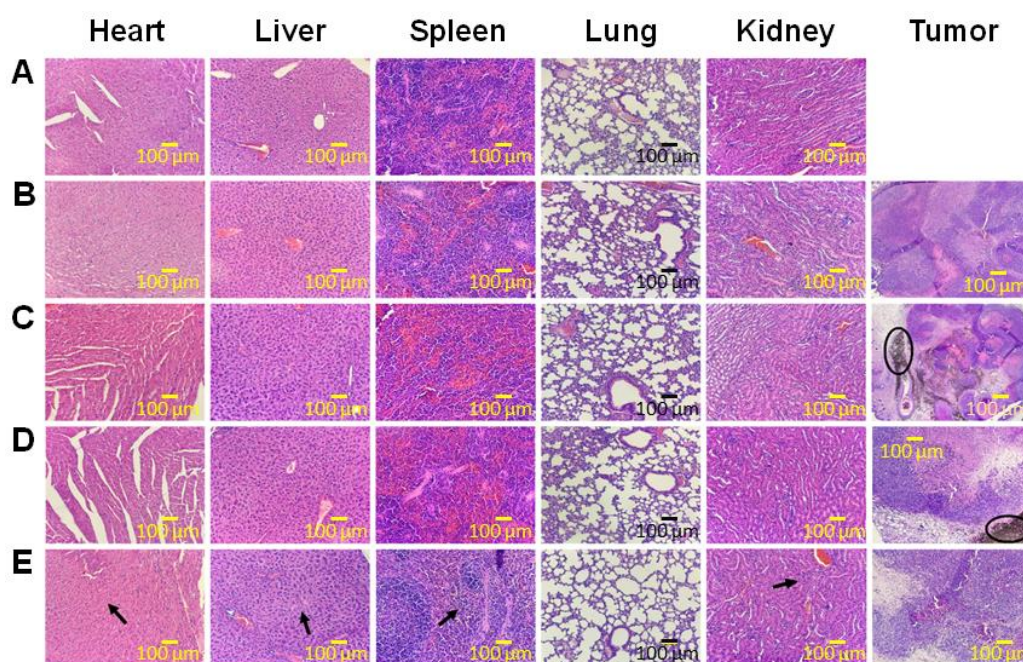
Fig. 7 Histopathological analysis of heart, liver, spleen, lung, and kidney sections isolated from healthy nude mice (A), and nude mice with established HeLa tumors after treatment with saline (B), NPFSSD (C), NPSSD (D) and free DOX(E), respectively. Images are representative mouse tissue sections stained with hematoxylin and eosin (H&E) and observed under a microscope at 200×magnification. Scale bars are calculated from the field of view, and added post-processing.

It is a limitation of the study that the injections were performed intratumorally. This does not measure the ability of the drug to localize to the tumour from general circulation, and additional studies would be required to determine localization efficacy. Consequently, although highly promising, these studies remain preliminary and further development remains underway.

Conclusions

We have designed a dual-gated triggerable theranostic nanodrug that exploits the overexpression of the folic acid receptor on cancer cells, and the higher endogenous levels of GSH in these cells, to control release and localize it to tumours. Although the use of the fluorescent DOX allowed for easy monitoring of the status of the drug, it is both fluorescently quenched and biologically inactive when covalently attached to the ND, there is no reason the same strategy could not be extended to any other therapeutic. As the drug is released primarily in the lysosome, it can readily migrate to the nucleus, evading normally effective resistance mechanisms that rely on pumping

642 the drug out as it diffuses into the cell, meaning this strategy could assist in extending

643 the useful life of chemotherapeutics against resistant tumors. The requirement for

644 elevated GSH levels and preferential uptake into folic acid receptor-overexpressing

645 cells, leads to selectivity and a decrease in the side effect profile of the drug. These

646 results are in agreement with previous reports.(DeFeo-Jones et al., 2000; Garsky et al.,

647 2001; Santra et al., 2011; Steendam et al., 2001; Zou et al., 2010)

648 Histopathological and biochemical analyses emphasize that free DOX is

649 hepatotoxic, while nanodrugs avoid this effect as the drug stays localized at the

650 tumour site. Hence, the strategy for the design of NPFSSD should be expandable for

651 the design of other endogenous species-specific triggers to drive the activation of

652 fluorescent and cytotoxicity. We believe that the NPFSS scaffold is a powerful, and

653 potentially universal, carrier for folate-receptor targeting and on-demand drug release,

654 with tremendous potential for clinical applications.

655

663

664 **Author Credit:** *Jiangtao Wu*: Methodology, Investigation, Resources, Data curation,

665 Writing-original draft. *Xiangbin Du*: Investigation, Resources, Methodology, Data

666 curation, Writing-original draft. *Dongmei Zhang*: Observation and analysis of tissue

667 section. *Jicheng Cui, Xiaoxia Zhang, Xine Duan*: Writing—Review and editing.

668 *John F. Trant*: Methodology, Writing—Review and Editing, Funding acquisition.

669 *Yingqi Li*: Methodology, Project administration, Supervision, Writing—review and

670 editing, Funding acquisition.

671

672 **References**

673   Ashrafizadeh, M., Saebfar, H., Gholami, M.H., Hushmandi, K., Zabolian, A.,
674 Bikarannejad, P., Hashemi, M., Daneshi, S., Mirzaei, S., Sharifi, E., Kumar, A.P.,
675 Khan, H., Heydari Sheikh Hossein, H., Vosough, M., Rabiee, N., Kumar Thakur, V.,
676 Makvandi, P., Mishra, Y.K., Tay, F.R., Wang, Y., Zarrabi, A., Orive, G., Mostafavi, E.,
677 2022. Doxorubicin-loaded graphene oxide nanocomposites in cancer medicine:
678 stimuli-responsive carriers, co-delivery and suppressing resistance. Expert Opin. Drug
679 Deliv. 19, 355-382.

680   Chauhan, S., Jain, N., Nagaich, U., 2020. Nanodiamonds with powerful ability
681 for drug delivery and biomedical applications: Recent updates on *in vivo* study and
682 patents. J. Pharm. Anal. 10, 1-12.

683   Cheng, R., Feng, F., Meng, F., Deng, C., Feijen, J., Zhong, Z., 2011.
684 Glutathione-responsive nano-vehicles as a promising platform for targeted
685 intracellular drug and gene delivery. J. Controlled Release 152, 2-12.

686   Cui, X., Liang, Z., Lu, J., Wang, X., Jia, F., Hu, Q., Xiao, X., Deng, X., Wu, Y.,
687 Sheng, W., 2021. A multifunctional nanodiamond-based nanoplatform for the
688 enhanced mild-temperature photothermal/chemo combination therapy of triple
689 negative breast cancer via an autophagy regulation strategy. Nanoscale 13,
690 13375-13389.

691   DeFeo-Jones, D., Garsky, V.M., Wong, B.K., Feng, D.-M., Bolyar, T., Haskell,
692 K., Kiefer, D.M., Leander, K., McAvoy, E., Lumma, P., Wai, J., Senderak, E.T.,
693 Motzel, S.L., Keenan, K., Zwieten, M.V., Lin, J.H., Freidinger, R., Huff, J., Oliff, A.,
694 Jones, R.E., 2000. A peptide–doxorubicin 'prodrug' activated by prostate-specific
695 antigen selectively kills prostate tumor cells positive for prostate-specific antigen *in*
696 *vivo*. Nat. Med. 6, 1248-1252.

697   Ding, Y., Dai, Y., Wu, M., Li, L., 2021. Glutathione-mediated nanomedicines for
698 cancer diagnosis and therapy. Chem. Eng. J. (Amsterdam, Neth.) 426, 128880.

699   Dong, Y., Cao, R.X., Li, Y.Q., Wang, Z.Q., Li, L., Tian, L., 2015.
700 Folate-conjugated nanodiamond for tumor-targeted drug delivery. RSC Adv. 5,
701 82711-82716.

702   Du, X.B., Li, L., Wei, S.G., Wang, S.B., Li, Y.Q., 2020. A tumor-targeted,
703 intracellular activatable and theranostic nanodiamond drug platform for strongly
704 enhanced *in vivo* antitumor therapy. J. Mat. Chem. B 8, 1660-1671.

705   Ferlay, J., Colombet, M., Soerjomataram, I., Parkin, D.M., Pineros, M., Znaor, A.,
706 Bray, F., 2021. Cancer statistics for the year 2020: An overview. Int. J. Cancer 149,
707 778-789.

708   Garsky, V.M., Lumma, P.K., Feng, D.-M., Wai, J., Ramjit, H.G., Sardana, M.K.,
709 Oliff, A., Jones, R.E., DeFeo-Jones, D., Freidinger, R.M., 2001. The synthesis of a
710 prodrug of doxorubicin designed to provide reduced systemic toxicity and greater
711 target efficacy. J. Med. Chem. 44, 4216-4224.

712   Hong, W., Guo, F., Yu, N., Ying, S., Lou, B., Wu, J., Gao, Y., Ji, X., Wang, H., Li,
713 A., Wang, G., Yang, G., 2021. A novel folic acid receptor-targeted drug delivery

714 system based on curcumin-loaded β-cyclodextrin nanoparticles for cancer treatment.
715 Drug design, development and therapy 15, 2843-2855.

716   Jiang, Y., Wickersham, K.E., Zhang, X., Barton, D.L., Farris, K.B., Krauss, J.C.,
717 Harris, M.R., 2019. Side effects, self-management activities, and adherence to oral
718 anticancer agents. Patient Prefer. Adherence 13, 2243-2252.

719   Jiao, J., Zhang, J., Yang, F., Song, W., Han, D., Wen, W., Qin, W., 2020. Quicker,
720 deeper and stronger imaging: A review of tumor-targeted, near-infrared fluorescent
721 dyes for fluorescence guided surgery in the preclinical and clinical stages. Eur. J.
722 Pharm. Biopharm. 152, 123-143.

723   Jung, H.-S., Neuman, K.C., 2021. Surface modification of fluorescent
724 nanodiamonds for biological applications. Nanomaterials 11, 153.

725   Lee, S.Y., Kang, M.S., Jeong, W.Y., Han, D.W., Kim, K.S., 2020. Hyaluronic
726 acid-based theranostic nanomedicines for targeted cancer therapy. Cancers (Basel) 12.

727   Li, L., Tian, L., Wang, Y., Zhao, W., Cheng, F., Li, Y., Yang, B., 2016. Smart
728 pH-responsive and high doxorubicin loading nanodiamond for *in vivo* selective
729 targeting, imaging, and enhancement of anticancer therapy. J. Mater. Chem. B 4,
730 5046-5058.

731   Li, T.-F., Xu, Y.-H., Li, K., Wang, C., Liu, X., Yue, Y., Chen, Z., Yuan, S.-J., Wen,
732 Y., Zhang, Q., Han, M., Komatsu, N., Zhao, L., Chen, X., 2019.
733 Doxorubicin-polyglycerol-nanodiamond composites stimulate glioblastoma cell
734 immunogenicity through activation of autophagy. Acta Biomater 86, 381-394.

735   Li, Y., Tong, Y., Cao, R., Tian, Z., Yang, B., Yang, P., 2014. *In vivo* enhancement
736 of anticancer therapy using bare or chemotherapeutic drug-bearing nanodiamond
737 particles. Int. J. Nanomed. 9, 1065-1082.

738   Li, Z., Tan, S., Li, S., Shen, Q., Wang, K., 2017. Cancer drug delivery in the nano
739 era: An overview and perspectives (Review). Oncology Reports 38, 611-624.

740   Ling, X., Chen, X., Riddell, I.A., Tao, W., Wang, J.Q., Hollett, G., Lippard, S.J.,
741 Farokhzad, O.C., Shi, J.J., Wu, J., 2018. Glutathione-scavenging poly(disulfide amide)
742 nanoparticles for the effective delivery of Pt(IV) prodrugs and reversal of cisplatin
743 resistance. Nano Lett. 18, 4618-4625.

744   Liu, K.-K., Cheng, C.-L., Chang, C.-C., Chao, J.-I., 2007. Biocompatible and
745 detectable carboxylated nanodiamond on human cell. Nanotechnology 18, 325102.

746   Liu, K.K., Zheng, W.W., Wang, C.C., Chiu, Y.C., Cheng, C.L., Lo, Y.S., Chen, C.,
747 Chao, J.I., 2010. Covalent linkage of nanodiamond-paclitaxel for drug delivery and
748 cancer therapy. Nanotechnology 21, 315106.

749   Long, W., Ouyang, H., Wan, W., Yan, W., Zhou, C., Huang, H., Liu, M., Zhang,
750 X., Feng, Y., Wei, Y., 2020. "Two in one": Simultaneous functionalization and DOX
751 loading for fabrication of nanodiamond-based pH responsive drug delivery system.
752 Mater. Sci. Eng. C 108, 110413.

753   Lv, Y., Xu, C., Zhao, X., Lin, C., Yang, X., Xin, X., Zhang, L., Qin, C., Han, X.,
754 Yang, L., He, W., Yin, L., 2018. Nanoplatform assembled from a CD44-targeted

prodrug and smart liposomes for dual targeting of tumor microenvironment and cancer cells. ACS Nano 12, 1519-1536.

Ma, Q., Zhang, Q., Yang, S., Yilihamu, A., Shi, M., Ouyang, B., Guan, X., Yang, S.-T., 2020. Toxicity of nanodiamonds to white rot fungi Phanerochaete chrysosporium through oxidative stress. Colloids Surf. B: Biointerf. 187, 110658.

Miller, K.D., Nogueira, L., Mariotto, A.B., Rowland, J.H., Yabroff, K.R., Alfano, C.M., Jemal, A., Kramer, J.L., Siegel, R.L., 2019. Cancer treatment and survivorship statistics, 2019. CA-Cancer J. Clin. 69, 363-385.

Mirzaei, S., Gholami, M.H., Hashemi, F., Zabolian, A., Farahani, M.V., Hushmandi, K., Zarrabi, A., Goldman, A., Ashrafizadeh, M., Orive, G., 2022. Advances in understanding the role of P-gp in doxorubicin resistance: Molecular pathways, therapeutic strategies, and prospects. Drug Discov. Today 27, 436-455.

Nicoletto, R.E., Ofner, C.M., 2022. Cytotoxic mechanisms of doxorubicin at clinically relevant concentrations in breast cancer cells. Cancer Chemother. Pharmacol. 89, 285-311.

Norouzi, P., Motasadizadeh, H., Atyabi, F., Dinarvand, R., Gholami, M., Farokhi, M., Shokrgozar, M.A., Mottaghitalab, F., 2021. Combination therapy of breast cancer by codelivery of doxorubicin and survivin siRNA using polyethylenimine modified silk fibroin nanoparticles. ACS Biomater. Sci. Eng. 7, 1074-1087.

Paris, J.L., Baeza, A., Vallet-Regí, M., 2019. Overcoming the stability, toxicity, and biodegradation challenges of tumor stimuli-responsive inorganic nanoparticles for delivery of cancer therapeutics. Expert Opin. Drug Deliv. 16, 1095-1112.

Pérez-Herrero, E., Fernández-Medarde, A., 2015. Advanced targeted therapies in cancer: Drug nanocarriers, the future of chemotherapy. Eur. J. Pharm. Biopharm. 93, 52-79.

Rahdar, A., Hajinezhad, M.R., Nasri, S., Beyzaei, H., Barani, M., Trant, J.F., 2020. The synthesis of methotrexate-loaded F127 microemulsions and their *in vivo* toxicity in a rat model. Journal of Molecular Liquids, 113449.

Santra, S., Kaittanis, C., Santiesteban, O.J., Perez, J.M., 2011. Cell-specific, activatable, and theranostic prodrug for dual-targeted cancer imaging and therapy. J. Am. Chem. Soc. 133, 16680-16688.

Sonju, J.J., Dahal, A., Singh, S.S., Gu, X., Johnson, W.D., Muthumula, C.M.R., Meyer, S.A., Jois, S.D., 2022. A pH-sensitive liposome formulation of a peptidomimetic-Dox conjugate for targeting HER2 + cancer. Int. J. Pharm. (Amsterdam, Neth.) 612, 121364.

Steendam, R., van Steenbergen, M.J., Hennink, W.E., Frijlink, H.W., Lerk, C.F., 2001. Effect of molecular weight and glass transition on relaxation and release behaviour of poly(dl-lactic acid) tablets. J. Controlled Release 70, 71-82.

Tu, Y.F., Peng, F., White, P.B., Wilson, D.A., 2017. Redox-sensitive stomatocyte nanomotors: Destruction and drug release in the presence of glutathione. Angew. Chem. Int. Ed. 56, 7620-7624.

796   Wang, L., Su, W., Ahmad, K.Z., Wang, X., Zhang, T., Yu, Y., Chow, E.K.-H., Ho,
797 D., Ding, X., 2022. Safety evaluation of nanodiamond-doxorubicin complexes in a
798 naïve Beagle canine model using hematologic, histological, and urine analysis. Nano
799 Res. 15, 3356-3366.

800   Wei, S.G., Li, L., Du, X.B., Li, Y.Q., 2019. OFF-ON nanodiamond drug platform
801 for targeted cancer imaging and therapy. J. Mat. Chem. B 7, 3390-3402.

802   Wu, Y., Alam, M.N.A., Balasubramanian, P., Ermakova, A., Fischer, S., Barth, H.,
803 Wagner, M., Raabe, M., Jelezko, F., Weil, T., 2021. Nanodiamond theranostic for
804 light-controlled intracellular heating and nanoscale temperature sensing. Nano Lett.
805 21, 3780-3788.

806   Xu, J., Gu, M., Hooi, L., Toh, T.B., Thng, D.K.H., Lim, J.J., Chow, E.K.-H.,
807 2021. Enhanced penetrative siRNA delivery by a nanodiamond drug delivery platform
808 against hepatocellular carcinoma 3D models. Nanoscale 13, 16131-16145.

809   Xu, Y., Shan, Y., Cong, H., Shen, Y., Yu, B., 2018. Advanced carbon-based
810 nanoplatforms combining drug delivery and thermal therapy for cancer treatment.
811 Curr. Pharm. Des. 24, 4060-4076.

812   Yang, G.L., Chen, C., Zhu, Y.C., Liu, Z.Y., Xue, Y.D., Zhong, S., Wang, C.C.,
813 Gao, Y., Zhang, W.A., 2019. GSH-activatable NIR nanoplatform with mitochondria
814 targeting for enhancing tumor-specific therapy. ACS Appl. Mater. Interf. 11,
815 44961-44969.

816   Yuan, S.-J., Wang, C., Xu, H.-Z., Liu, Y., Zheng, M.-Y., Li, K., Sun, S.-K.,
817 Komatsu, N., Zhao, L., Chen, X., 2021. Conjugation with nanodiamonds via
818 hydrazone bond fundamentally alters intracellular distribution and activity of
819 doxorubicin. Int. J. Pharm. (Amsterdam, Neth.) 606, 120872.

820   Zhang, J., Wang, L., Fai Chan, H., Xie, W., Chen, S., He, C., Wang, Y., Chen, M.,
821 2017. Co-delivery of paclitaxel and tetrandrine via iRGD peptide conjugated
822 lipid-polymer hybrid nanoparticles overcome multidrug resistance in cancer cells. Sci.
823 Rep. 7, 46057.

824   Zhang, X.-Q., Lam, R., Xu, X., Chow, E.K., Kim, H.-J., Ho, D., 2011.
825 Multimodal nanodiamond drug delivery carriers for selective targeting, imaging, and
826 enhanced chemotherapeutic efficacy. Adv. Mater. 23, 4770-4775.

827   Zhao, G.F., Sun, Y., Dong, X.Y., 2020. Zwitterionic polymer micelles with dual
828 conjugation of doxorubicin and curcumin: Synergistically enhanced efficacy against
829 multidrug-resistant tumor cells. Langmuir 36, 2383-2395.

830   Zhao, L., Xu, Y.-H., Akasaka, T., Abe, S., Komatsu, N., Watari, F., Chen, X.,
831 2014. Polyglycerol-coated nanodiamond as a macrophage-evading platform for
832 selective drug delivery in cancer cells. Biomaterials 35, 5393-5406.

833   Zou, P., Yu, Y., Wang, Y.A., Zhong, Y., Welton, A., Galbán, C., Wang, S., Sun, D.,
834 2010. Superparamagnetic iron oxide nanotheranostics for targeted cancer cell imaging
835 and pH-dependent intracellular drug release. Mol. Pharmaceutics 7, 1974-1984.

836